March 2019

Structure Beneath the Northern Los Angeles Basins from Teleseismic Receiver Functions

Guibao Liu
Louisiana State University and Agricultural and Mechanical College

STRUCTURE BENEATH THE NORTHERN LOS ANGELES BASINS FROM TELESEISMIC RECEIVER FUNCTIONS

A Thesis

Submitted to the Graduate Faculty of the
Louisiana State University and
Agricultural and Mechanical College
in partial fulfillment of the
requirements for the degree of
Master of Science

in

The Department of Geology and Geophysics

by
Guibao Liu
B. E., Ocean University of China, 2005
M. E., RIPED, 2008
May 2019

Table of Contents

Acknowledgements

I would like to thank Dr. Persaud, acting as my major professor, who offered me the opportunity to participate a very exciting project that employs the nodal seismic data and the well-established teleseismic receiver function method to investigate the structurally complicated northern Los Angeles basins. She provided me the required data sets, which she collected in the Los Angeles urban area, and the codes for calculating receiver functions, which is proven very robust in this study. During the project, she also provided me a lot of inspiring ideas about how to tackle many difficult issues in my research. In particular, her edition on the manuscript significantly improved it and made possible its publication.

I would thank my other committee members, Dr. Juan Lorenzo, and Dr. Karen Luttrell who provided me many invaluable suggestions on how to improve my research and this thesis. Their advice significantly enhances this thesis. Thank Dr. Lorenzo and his students, Daniel and Aba, who help improve my presentation. Thank you all!

I would also thank the Department of Geology and Geophysics that hosts me as a graduate student and offers me a teaching assistantship. The departmental administration and staff, Dr. Brooks Ellwood, Lori Bond, Rachel May, Sonja Scott, Jeffrey Springer, and et al., are always ready to reach out when I am experiencing tough situations.

I would thank all the faulty members who taught me in classroom and for whom I worked as a TA. The selected courses solidify and broaden my knowledge in geosciences. Working as a TA offers me a unique perspective of observing how to instruct students while I am able to participate the instructions. In addition, I am often inspired by the knowledge I learned in the TA classes.

I would like to thank the journal Seismological Research Letters for the permission of letting me build my thesis on my paper they have published.

Finally, I thank my family and my parents, who always support me no matter what situations I am in. Their love and support enable me enduring and dealing with all kinds of difficulties with peace and joy. Hereby, I dedicate this thesis to them.

Abstract

This thesis presents part of the work published in Liu et al. (2018).

The Los Angeles area is at high risk of seismic amplification due to its location on top of sedimentary basins. It is very important to obtain accurate information on the crustal structure, in particular, the basin structure of the northern basins, in order to estimate the resulting ground motion and earthquake hazards due to a large San Andreas fault earthquake. In the Liu et al. (2018) study, we image the crustal structure beneath the northern basins using a densely spaced, autonomous 3-component seismometer array in the urban Los Angeles area.

Using the collected nodal data, the receiver function technique was applied to image the crustal and basin structure. First, the nodal waveforms are compared to nearby broadband data to confirm that the nodal data is suitable for receiver function calculation. Second, receiver functions are computed from the nodal datasets and compared to those from broadband recordings. Third, the nodal receiver functions are interpreted to help characterize the crustal structure beneath the northern basins.

1. Introduction

The paper (Liu et al., 2018) summarizes my graduate work, which aims to reveal the crustal structure beneath the northern Los Angeles basins using teleseismic receiver functions calculated from nodal seismic waveforms. A more complete explanation of this work is presented in Liu et al. (2018).

This thesis mainly contains three parts. Section 1 presents a brief introduction to the structure of the thesis. The following sections describe the research I have conducted, including geologic setting, previous work, the receiver function method, the interpretation approaches, limitations and uncertainties of the work, and brief discussion and conclusions of the work. Finally, an appendix presents a list of the directory structure and files used for calculating the receiver functions in the paper. Other items in this study, such as processing schemes, data set, and detailed results and discussion are presented in the paper by Liu et al. (2018).

2. Geologic Setting

The greater Los Angeles region is geologically located in a transitional segment of the broad San Andreas transform fault zone (Figure 1), where, to the south, lies the Peninsular Ranges dominated by right-lateral strike-slip tectonics while to the north, lies the Transvers Ranges with folding and contractional faulting (e.g. Walls et al., 1998; Yeats, 2004). This area contains several sedimentary basins, like the Los Angeles basin, the San Gabriel basin, and the San Bernardino basin. The region is shaped by multiple periods of deformations including Cretaceous –early-Paleogene subduction, Paleogene terrane accretion, Miocene extension, Pliocene contraction, and Plio-Quaternary transpression (e. g., Luyendyk, 1991; Wright, 1991; Dickinson, 1996; Walls et al., 1998). Meanwhile, because it is located near the big bend of the San Andreas Fault system, this region is also situated in a very complex stress field, with approximately N-S striking maximum principal stresses (Walls et al., 1998; Hauksson, 1990; Mount and Suppe, 1992) and N-S shortening rate of 7-9 mm/yr across the Los Angeles area based on geodetic observations (Walls et al., 1998).

The study area is the northern basins (Figures 1 and 2) which are bounded by San Gabriel Mountains to the north, the Repetto and Montebello Hill to the west (Yeats, 2004), the Whittier Fault and the Peninsular Ranges to the south, and the San Andreas Fault to the east. The nodal deployments cross or are adjacent to several faults (certain or inferred). For example, the Raymond fault (RF in Figure 2) has been interpreted as having a left-lateral slip fault, and it strikes roughly east-west and connects with the Sierra Madre fault to the east. (Yeats, 2004). Northeast-trending within the San Bernardino basin, the Red Hill-Etiwanda Avenue fault (RH in Figure 2) is an inferred active left-lateral strike-slip fault based on micro-earthquakes (Cramer and Harrington, 1980).

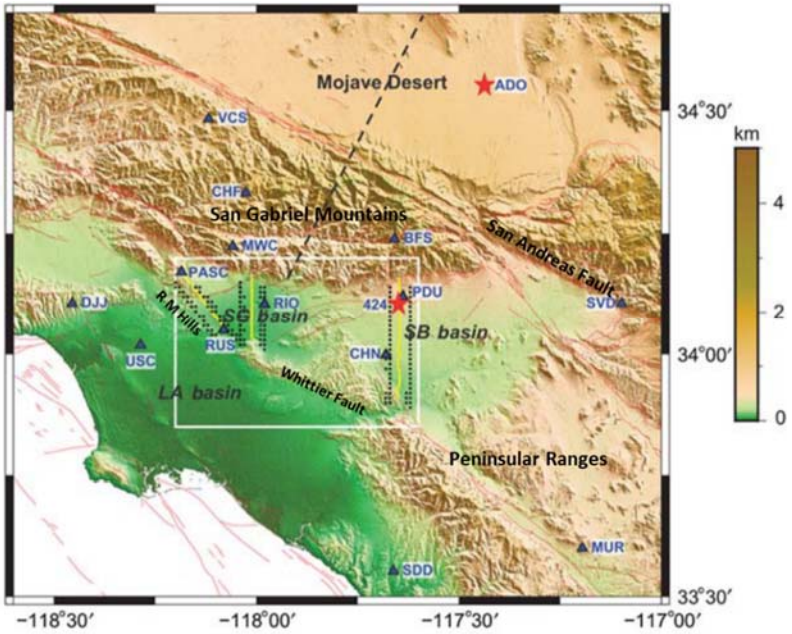

Figure 1. Map of the study area. R M Hills: The Repetto and Montebello Hills. (modified from Fig. 1a in Liu et al., 2018; Labels for R M Hills, Whitter Fault, Peninsular Ranges, and San Andreas Fault were added)

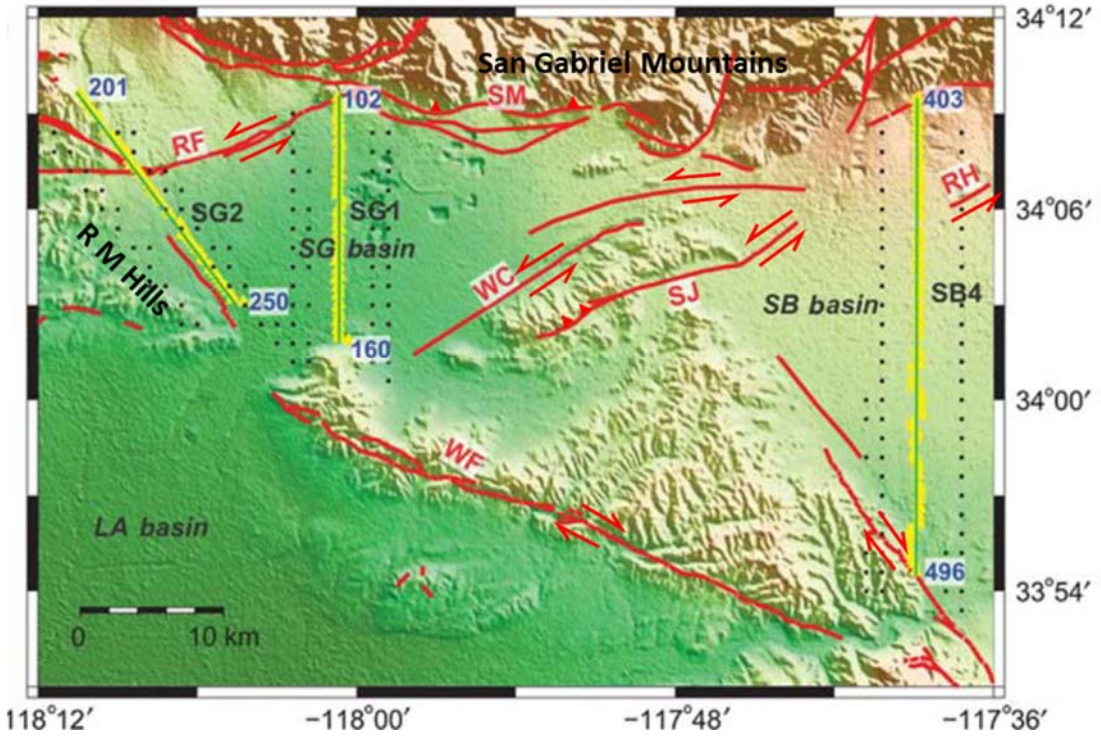

Figure 2. An expanded map of the study area. Annotations are explained on Fig. 1b in Liu et al. (2018) (modified from Fig. 1b in Liu et al., 2018; Labels for RM Hills and San Gabriel Mountains were added)

3. Previous Work

As summarized from Liu et al. (2018), one of the previous studies obtaining estimates of the basement depths in the Greater Los Angeles area was carried out by modeling gravity and aeromagnetic data to determine the basin floor of the San Bernardino basin (Anderson et al., 2004). That work provides the basement structure in three dimensions, but the basement map in the basin is of low resolution due to the sparse gravity control points (Figure 3).

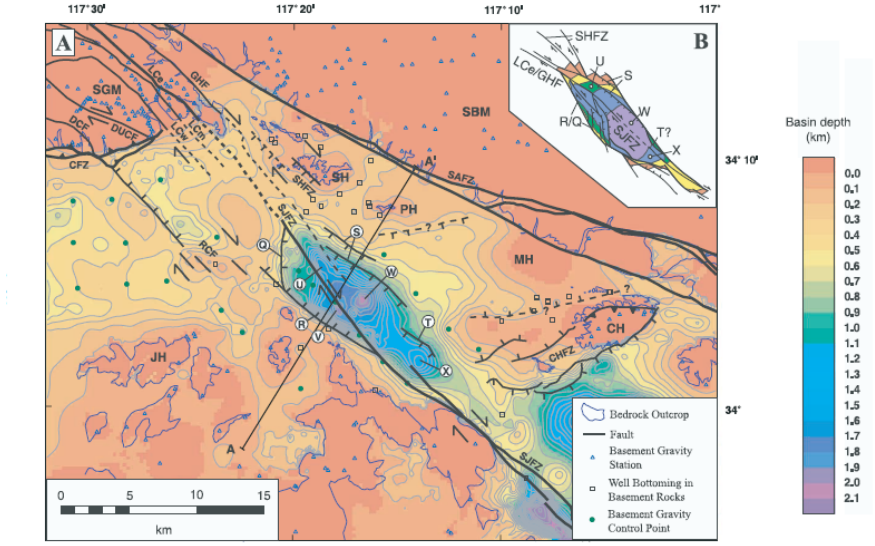

Figure 3. The basin floor depth map with an overall horizontal resolution of 1 km (Fig. 5 in Anderson et al., 2004)

Magistrale et al. (2000) produced velocity models for the major southern California basins by combining geotechnical data and Faust's empirical equation for obtaining V_P from sediment age and depth. The well locations and geotechnical boreholes are sparse which significantly affect the spatial resolution of the model, in particular, in our study area.

Another effort to study of the basin structure in the greater Los Angeles region was conducted by Süss and Shaw (2003) who produced a 3-D P-wave seismic velocity model using a

geostatistical approach by integrating the velocities derived from sonic well logs and those from the seismic stacking. However, the sparsely distributed well logs and seismic reflection datasets limited the spatial resolution of the model in the northern basins.

In the Los Angeles Region Seismic Experiment (LARSE), a seismic refraction and low-fold reflection survey, one deployment was conducted cross the San Gabriel basin, which was able to provide a detailed velocity section of the San Gabriel basin. (Fuis et al., 1996; Fuis et al., 2001). However, only one interpreted cross-section was presented across the San Gabriel basin. Similarly, the study by Yeats (2004) offered little information about the shape of the northern basins.

Seismic tomography has been frequently employed, e.g., to construct the SCEC Community Velocity Models (e.g., Tape et al., 2009; Lee et al., 2014). The CVMs show the shape and structure of the northern basins at a large scale.

In the northern basins, Zhu and Kanamori (2000) mapped the Moho depths in southern California using broadband receiver functions, which also covered the northern basins. But the lateral resolution is limited by the spacing of the broadband stations. Similarly, a Moho depth map of the southern California was provided by Yan and Clayton (2007). Zhu (2000) constructed crustal profiles of receiver functions to the west of the northern basins. His results are compared with the results in this study. Ma and Clayton (2016) partially reveal the basement of the San Gabriel basin using receiver functions calculated from LASSIE dense broadband arrays.

To sum up, the previous studies provide the crustal and basin structure of the northern basins at a regional scale. Our nodal receiver function arrays image the structure of the northern basins along three profiles.

4. Method

The receiver function technique has already developed into a routine method in seismic imaging approaches. Because receiver functions are sensitive to the variation of the subsurface structure, they are frequently applied to study crustal interfaces, Moho discontinuity, or mantle interfaces (e.g., Zhu. 2000). In this study, the P wave receiver functions are primarily used to investigate the basin and crustal structure. The receiver functions mentioned in the following text are referred to P wave receiver functions. In addition, I would follow Langston's work to explain the principles of receiver functions (Langston, 1979).

The three components seismic data have to be rotated to the vertical component (V), the radial component (R), and the tangential component (T), prior to calculating receiver functions. A receiver function is a time series calculated by deconvolving the vertical component from radial or tangential components of a 3-component seismograph.

Using Langston's notations and the analysis presented in that study (Langston, 1979), the three components (V, R, T) of the teleseismic P wave waveforms are represented as follows:

$D_V(t) = I(t) * S(t) * E_V(t)$ ……Eq. 1

$D_R(t) = I(t) * S(t) * E_R(t)$ ……Eq. 2

$D_T(t) = I(t) * S(t) * E_T(t)$ ……Eq. 3

where, $D_V(t)$ is the vertical component, $D_R(t)$ indicates the radial component, and $D_T(t)$ presents the tangential component. $I(t)$ indicates the instrument response of the seismic station, which is assumed to be the same for all the three components. $E_V(t)$, $E_R(t)$, and $E_T(t)$ are the crust and/or mantle transfer functions for the three component recordings, respectively. $S(t)$ is the teleseismic source function.

Based on observations, Langston (1979) found that $E_V(t)$ behaves like a Dirac delta function and therefore, assumes that:

$D_V(t) = I(t) * S(t)$ … ……Eq. 4

Subsequently, Eq. 2 and Eq. 3, the radial and tangential components, can be written in the following forms:

$D_R(t) = D_V(t) * E_R(t)$ ……Eq. 5

$D_T(t) = D_V(t) * E_T(t)$ ……Eq. 6

Or in the frequency domain:

$D_R(w) = D_V(w)E_R(w)$ ……Eq. 7

$D_T(w) = D_V(w)E_T(w)$ ……Eq. 8

Then,

$E_R(w) = \frac{D_R(w)}{D_V(w)}$ ……Eq. 9

$E_T(w) = \frac{D_T(w)}{D_V(w)}$ ……Eq. 10

Eq. 9 and Eq. 10 are the radial and tangential receiver functions in frequency domain, respectively.

Receiver functions can be calculated by deconvolution in the time domain or the frequency domain. For instance, Langton (1979) calculated receiver functions using a method of deconvolution in the frequency domain developed by Helmberger and Wiggins (1971) and Dey-Sarkar and Wiggins (1976b). In the time domain, the iterative time-domain deconvolution is also frequently used for receiver function calculation (e.g., Ligorría and Ammon, 1999). In this study, we use a frequency domain deconvolution (Oldenburg, 1981) to calculate receiver functions using teleseismic arrivals from 4 earthquakes at 15 broadband stations and ~ 200 nodes (please see Liu et al., 2018, for complete details).

5. Interpretation Approaches

This section serves as an explanation of how the interpretation of receiver functions is conducted. Determining all the conversions on the receiver function profiles, like Moho conversions, is actually a critical step for the interpretations in this study. I conducted and solidified the interpretations through multiple approaches and multiple sources of information.

The interpretations of the Moho are based on calculations and also intensively referred to previous studies, in particular, the work of Zhu (2000) on estimating Moho depth in southern California from teleseismic receiver functions. According to Zhu's results, the Moho depth in the southern California varies from 21 to 37 km with an average value of 29 km. The arrivals of Moho conversion in receiver functions can be predicted by the following equation:

$$t_{P_s} = H * \left(\sqrt{\frac{1}{V_s^2} - p^2} - \sqrt{\frac{1}{V_p^2} - p^2}\right) \quad \text{Eq. 11}$$

(Zhu and Kanamori, 2000)

where, t_{P_s} is the time difference between Moho Ps and P arrival, H is the Moho depth, Vp and Vs are the seismic velocity in crust. If the Moho depth is assumed to be 30 km, the ray parameter p is 0.051, Vp is constant at 6.3 km/s, while k, the ratio of Vp and Vs, is 1.73, 1.8, or 1.9, t_{P_s}, the predicted time differences between P and the Moho Ps calculated with Eq. 11 are listed in Table 1.

Taking into account the calculations of the predicted time difference between P and Moho Ps, 4 seconds is a reasonable value for the Moho conversions, on average. This value is what I am using in the interpretation of the Moho discontinuity. The Moho depth is also verified by Zhu's work on the crustal structure based on LARSE-93 deployments (Zhu, 2000). His results

are shown in Figure 4, where the stacked receiver functions reveal the depths and relief of the Moho discontinuity beneath the region that is near to our study area.

Table 1. The predicted time difference between P and Moho Ps

Moho Depth (km)	Vp (km/s)	p (s/km)	Vs (km/s)	k	tps (s)
30	6.3	0.051	3.64	1.73	3.60
30	6.3	0.051	3.50	1.8	3.92
30	6.3	0.051	3.32	1.9	4.41

The initial interpretations are also carried out based on the consistency and coherency in the conversions. Coherent conversions are interpreted as a continuous Moho discontinuity while abrupt breaks in the conversions are likely related to possible faults. Given that the close intervals of the nodal seismometers, an abrupt change in the continuous conversion event is more likely caused by a fault. In addition, the interpretations of inferred faults are also based on the evidence of existing faults in the northern basins. If there is existing a fault close to the interpreted offset, a correlation would be drawn between them. Moreover, the regional geologic and tectonic settings are also considered to make sense all the interpretations.

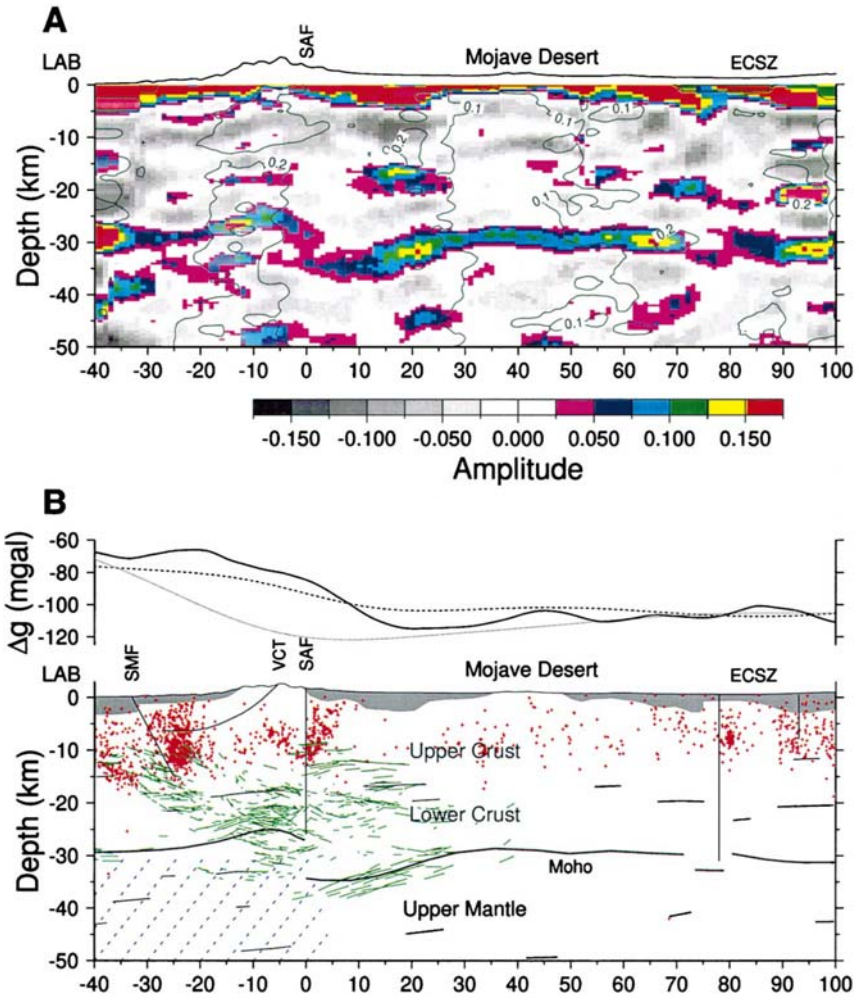

Figure 4. The crustal structure from Mojave Desert to the San Gabriel basin (Fig.3 in Zhu, 2000)

The intra-basin conversions are checked after initial interpretations by calculating the estimated basement depths beneath the northern basins. In order to rule out that the interpreted intra-crustal interfaces or Moho discontinuity might be the multiples of the basement conversions, I chose two control points for each line to calculate the predicted multiples of the basement conversions. Figure 5 shows the interpretation.

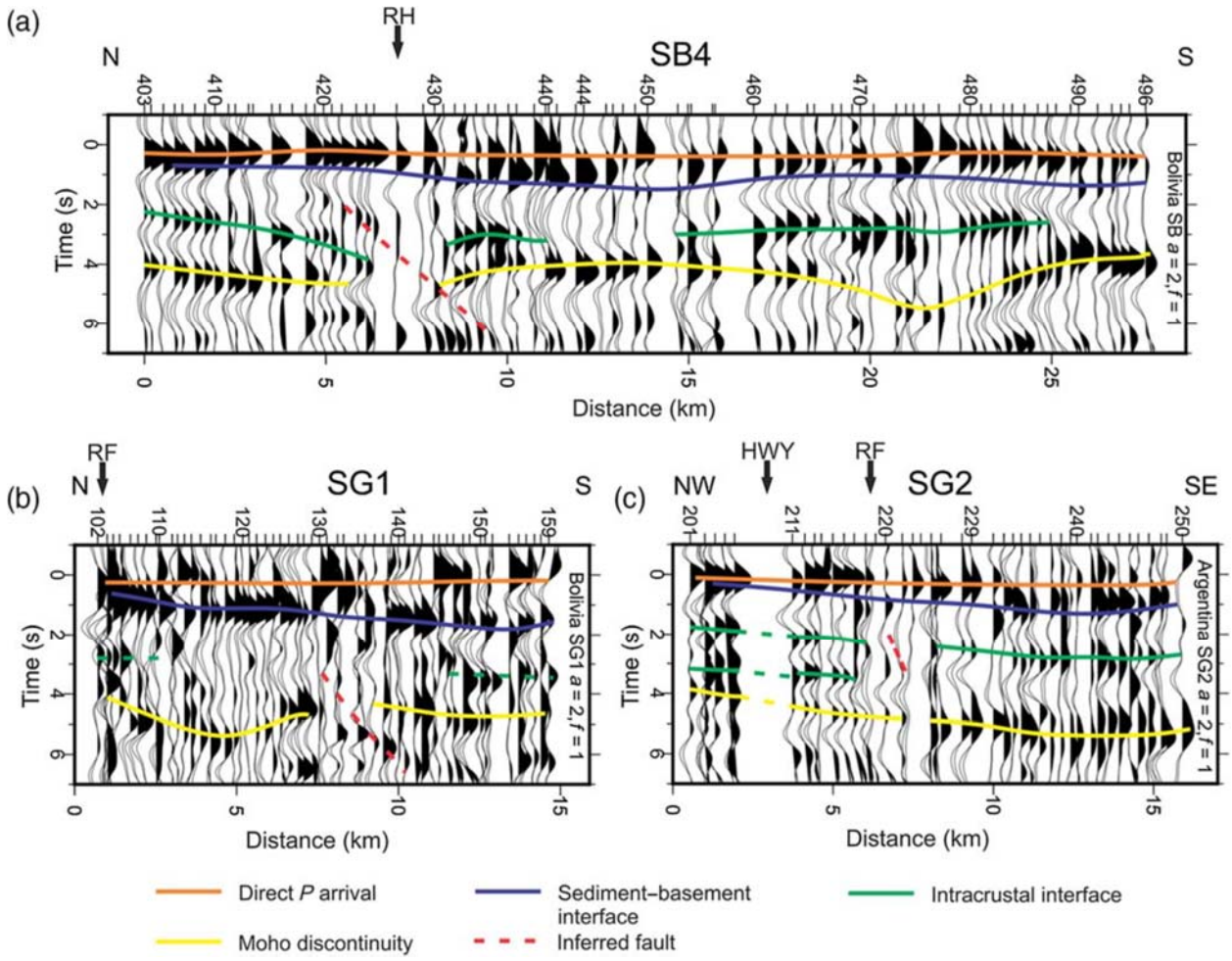

Figure 5. The interpretation of ~1 Hz receiver functions (Fig. 5 in Liu et al., 2018)

The differential times of P and Ps are read from the receiver function profiles directly. Vs and Vp are the seismic velocities of sediments determined from the literature review. The predicted differential times for multiple are calculated with equations provided in Zhu and Kanamori (2000).

Ray parameter p is the average value of all the nodal geophones. Predicted P_PP_S and P_PS_S/P_SP_S are the possible times for the multiples of the basement conversions while the intra-crustal depth and Moho depth are read from the interpreted profiles. Comparing the values of predicted times of multiples, intra-crustal depth, and Moho depth, it is concluded that the

interpreted intra-crustal interfaces and Moho discontinuity are not the multiples of the basement conversions.

The broadband receiver functions that were calculated in this study and the receiver functions calculated by Zhu (2000) were compared when determining the conversions of the Moho discontinuity and intra-crustal interfaces (Figure 6). In addition, the Moho and intra-crustal conversions are compared among nodal receiver functions of different frequencies (Figure 7). The crustal conversions in different profiles are almost identical.

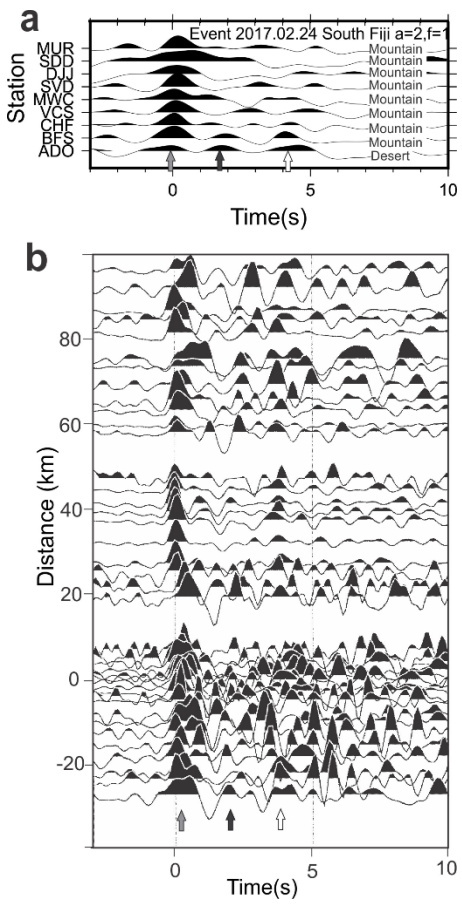

Figure 6. Crustal structure revealed by broadband receiver functions, a. the neighboring broadband receiver functions, b. the receiver functions calculated by Zhu (2000). Gray arrows: the direct P arrival; Black arrows: the intra-crustal Ps conversion; White arrows: the Moho Ps conversion. (modified from Fig. 4 in Liu et al., 2018; only broadband receiver functions were kept)

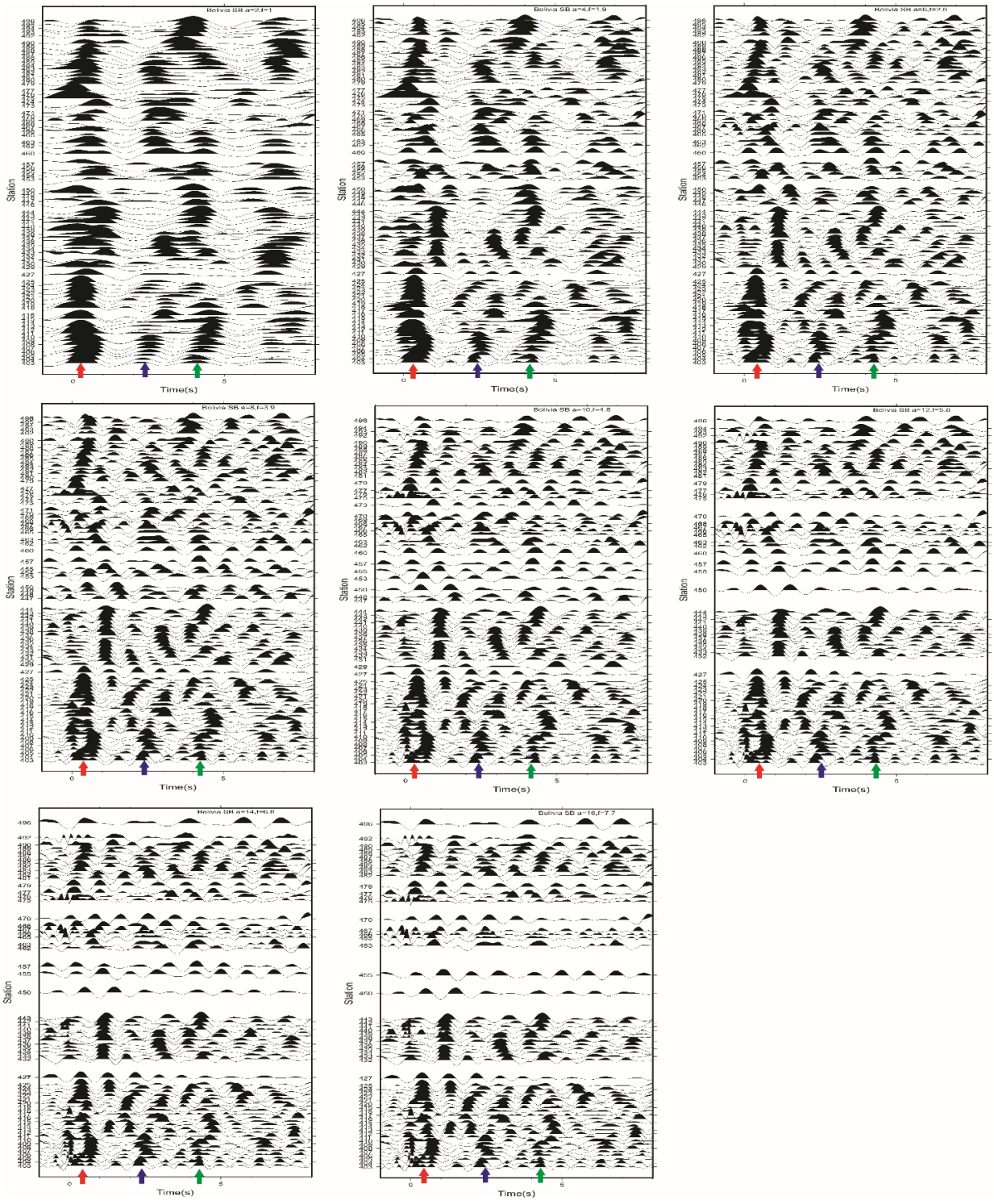

Figure 7. Nodal receiver functions of SB4 line, for one event, with different Gaussian parameter. Red arrows: the direct P arrival; Blue arrows: the intra-crustal Ps conversion; Green arrows: the Moho Ps conversion.

6. Limitations and Uncertainties

As explained in Liu et al. (2018), although receiver functions are frequently used in the investigation of deep earth structure, they are not always produced robustly when the seismic recordings are collected on top of the sediments (e.g., Yeck et al., 2013; Yu et al., 2015). The interference effect caused by sediments may also be observed in the nodal receiver function profiles. The inference may actually affect the accuracy of the geologic interpretation. In the future receiver function studies in sedimentary basins, the inference resulting from sediments should be handled, in some ways like the sequential H-κ stacking proposed by Yeck et al. (2013) or the resonance removal filtering suggested by Yu et al. (2015).

In this study, the receiver function profiles are directly interpreted in time domain. Conventionally, the receiver functions are migrated or CCP stacked, in which the receiver functions are converted into the depth domain. The receiver functions are not migrated either in order to avoid any possibility of bringing additional error or inaccuracy from inappropriate velocity models that are employed in migration, which is the advantage of time domain interpretation. But, the interpretation in time domain may be difficult in determining the dip angles of inferred faults, estimating the “true” basement depths and Moho relief. In the future research, the nodal receiver functions could still be converted into the depth domain by appropriate approaches.

7. Summary of workflow and results

The computation of the receiver functions was done with the codes and a manual provided by Dr. Persaud, following steps and methods that were tested and developed by Dr. Persaud and collaborators. In this part, my contribution to this paper is as follows:

1) Set up the working directory for receiver function calculations and build up a set of procedures for calculating nodal receiver functions.

2) During the calculation of nodal and broadband receiver functions, additional shell scripts are developed to facilitate the processing of raw waveforms, like fixing the SAC headers, modifying the file names, prepping the event files for receiver function calculations.

3) Develop scripts in SAC, GMT, and Linux Shell, in order to plot and compare the waveforms and receiver functions of nodal and broadband data sets. The spectral comparisons are done in SAC, while the waveforms are plotted and then compared using GMT and Linux scripts.

4) The receiver functions are plotted primary using pssac in GMT , either by uniform spacing intervals, or by real projected distance along the profile.

5) Calculate the nodal and neighboring broadband receiver functions for the comparison purposes. The calculated receiver functions are compared to the previous results, e.g., the LARSE-93 (Zhu, 2000).

6) Calculate nodal receiver functions based on all the selected events and all the nodal datasets, with different Gaussian parameters, from 2, 4, up to 16.

7) Interpret the selected receiver function profiles of low and high frequency, combining the information of regional tectonics, previous work, and various calculations.

8) Complete a draft manuscript.

8. Discussion and conclusions

This serves as a brief summary of the paper by Liu et al. (2018).

In this study, we explored the use of three-component nodal seismic datasets, collected by dense geophone arrays in crustal studies of the northern basins in the greater Los Angeles area. By comparing the nodal waveforms to neighboring broadband recordings, we found the nodal seismic data consist of sufficient signal content for producing receiver functions. The receiver functions calculated from nodal recordings are subsequently employed in the interpretation of the crustal structure beneath the northern basins. Through this study, we reach the following conclusions.

First, according to the comparisons of waveforms and spectral characteristics between nodal and broadband seismograms, the nodal seismic data sets contain sufficient frequency bandwidth to produce teleseismic receiver functions.

Second, the calculated receiver functions from nodal data and neighboring broadband stations, reveal similar subsurface features, like intra-crustal interfaces and Moho discontinuity beneath the northern basins. In addition, nodal receiver function arrays are capable of providing more continuous crustal structures because of the dense spacing that is possible with the nodal geophones and relatively higher frequency content in nodal receiver functions.

Third, the basin shape and crustal structure beneath the northern basins are revealed by the nodal receiver function profiles. The basin shape and structure would help improve the subsequent assessment of earthquake hazard in the Los Angeles metropolitan area.

Fourth, three possible deep faults are interpreted and two of them may be related to neighboring documented faults. Along the SB4 profile, the interpreted offset is close to the surface trace of the Red Hill-Etiwanda Avenue Fault located in the northern part of the San

Bernardino basin. In the SG2 profile, the surface projection of the inferred fault is close to the Raymond Fault.

Fifth, this study demonstrates that nodal seismometer arrays have great potential in the imaging of crustal structure. Moreover, nodal deployments would make possible the integration of the well-established signal processing and imaging techniques used in reflection seismology.

Bibliography

Anderson, M., Matti, J., and Jachens, R., 2004, Structural model of the San Bernardino basin, California, from analysis of gravity, aeromagnetic, and seismicity data, *J. Geophys. Res*. **109**, no. B4, DOI: doi:10.1029/2003JB002544.

Cramer, C and J. Harrington (1980). Seismicity and Tectonics of the Cucamonga Fault and the Eastern San Gabriel Mountains, San Bernardino County in *Recent reverse faulting in the Transverse Ranges, California, USGS Professional Paper* **1339**, 7-26.

Dey-Sarkar, S. K., and R. A. Wiggins (1976b). Source deconvolution of teleseismic P wave arrivals between 14° and 40°, *J. Geophys. Res*., **81**, 3633-3641.

Di Bona, M. (1998). Variance estimate in frequency-domain deconvolution for tele-seismic receiver function computation*, Geophys. J. Int.* **134**, 634-646.

Dickinson, W. (1996). Kinematics of transrotational tectonism in the California Transverse Ranges and its contribution to cumulative slip along the San Andreas transform fault system, Geol. Soc. Am. Spec. Pap. 305, 1–50.

Fuis, G. S., D.A. Okaya, R. W. Clayton, W.J. Lutter, T. Ryberg, T. M. Brocher, T. L. Henyey, Benthien, M.L., Davis, P.M., Mori, J., Catchings, R.D., tenBrink, U.S., Kohler, M.D., Klitgord, K.D., and Bohannon, R.G. (1996). Images of crust beneath southern California will aid study of earthquakes and their effects: *Eos (Transactions, American Geophysical Union)* **77**, p. 173, 176.

Fuis, G.S., T. Ryberg, N.J. Godfrey, D.A. Okaya, and J. M. Murphy (2001). Crustal structure and tectonics from the Los Angeles Basin to the Mojave Desert, southern California, *Geology* **29**, p. 15–18.

Hauksson, E (1990). Earthquakes, faulting, and stress in the Los Angeles Basin. *J. Geophys. Res*. **95**, 15365–15394.

Helmberger, D., and R. A. Wiggins (1971). Upper mantle structure of Midwestern United States, *J. Geophys. Res*., **76**, 3229-3245.

Jennings, C.W., and W.A. Bryant (2010), Fault activity map of California, *California Geological Survey Geologic Data Map* **6**, scale 1: 750,000.

Juan Pablo Ligorría, Charles J. Ammon (1999). Iterative deconvolution and receiver-function estimation. *Bull. Seismol. Soc. Am.* **89** (5), 1395–1400.

Kennett, B.L.N. (Compiler and Editor). 1991. *IASPEI 1991 Seismological Tables*, Bibliotech, Canberra, Australia, 167 pp.

Langston, C.A. (1979). Structure under Mount Rainier, Washington, inferred from tele-seismic body waves, *J. Geophys. Res.* **84**, 4749-4762.

Lee, E. J., P. Chen, T. H. Jordan, P. B. Maechling, M. A. M. Denolle, and G. C. Beroza (2014). Full-3-D tomography for crustal structure in Southern California based on the scattering-integral and the adjoint-wavefield methods, *J. Geophys. Res. Solid Earth.* **119**, 6421-6451, doi:10.1002/2014JB011346.

Liu, G., P. Persaud, and R. W. Clayton (2018). Structure of the Northern Los Angeles Basins Revealed in Teleseismic Receiver Functions from Short-term Nodal Seismic Arrays, *Seismol. Res. Lett.* **89**, 1680–1689, https://doi.org/10.1785/0220180071.

Luyendyk, B (1991). A model for Neogene crustal rotations, transtension, and transpression in southern California. *Geol. Soc. Am. Bull*. **103**, 1528–1536.

Ma, Y. and R. Clayton (2016). Structure of the Los Angeles Basin from ambient noise and receiver functions, *Geophys. J. Int.* **206**, 1645-1651, doi:10.1093/gji/ggw236.

Magistrale, H., S. Day, R. W. Clayton, and R. Graves (2000). The SCEC Southern California reference three-dimensional velocity model Version 2, *Bull. Seismol. Soc. Am*., **90** (6B), S65-S76.

Mount, S. and J. Suppe (1992). Present-day stress orientations adjacent to active strike-slip faults, California and Sumatra. *J. Geophys. Res*. **97**, 11995–12103.

Oldenburg, D. W. (1981). A comprehensive solution to the linear deconvolution problem. *Geophys. J. R. astr. Soc.* **65**, 331-357, doi:10.1111/j.1365-246X.1981.tb02716. x.

Ryberg, T. and M. Weber (2000). Receiver function arrays: a reflection seismic approach, *Geophys. J. Int.* **141**, 1-11.

Süss, M. P., and J. H. Shaw (2003). P-wave seismic velocity structure derived from sonic logs and industry reflection data in the Los Angeles basin, California, J. Geophys. Res., **108** (B3), 2170, doi:10.1029/2001JB001628.

Tape, C., Q. Liu, A. Maggi, and J. Tromp (2009). Adjoint tomography of the southern California crust, *Science* **325**, 988–992.

Walls, C., T. K. Rockwell, K. J. Mueller, Y. Bock, S. Williams, J. L. Pfanner, J. F. Dolan, and P. Fang (1998). Escape Tectonics in the Los Angeles Metropolitan Region and the Implications for Seismic Risk. *Nature*, **394**, 356-360. doi: 10.1038/28590.

Ward, K and F. Lin (2017). On the Viability of Using Autonomous Three-Component Nodal Geophones to Calculate Tele-seismic Ps Receiver Functions with an Application to Old Faithful, Yellowstone, *Seismol. Res. Lett.* **88** (5), 1268-1278, doi: 10.1785/0220170051.

Wright, T.L. (1991). Structural geology and tectonic evolution of the Los Angeles Basin, in Biddle, K.T., ed., Active margin basins: *American Association of Petroleum Geologists Memoir* **52**, p. 35–134.

Yan, Z. and R. Clayton (2007). Regional mapping of the crustal structure in southern California from receiver functions, *J. Geophys. Res*. **112,** B05311. doi:10.1029/2006JB004622.

Yeats, R.S. (2004). Tectonics of the San Gabriel Basin and surroundings, southern California. *GSA Bulletin* **116** (9-10): 1158–1182. doi: https://doi.org/10.1130/B25346.1

Yeck, W. L., A. F. Sheehan, and V. Schulte-Pelkum (2013). Sequential H-k stacking to obtain accurate crustal thicknesses beneath sedimentary basins, *Bull. Seismol. Soc. Am.* **103**, 2142-2150.

Yu, Y., J. Song, K. H. Liu, and S. S. Gao (2015). Determining crustal structure beneath seismic stations overlying a low-velocity sedimentary layer using receiver functions, *J. Geophys. Res. Solid Earth* **120**, 3208-3218.

Zhu, L. (2000). Crustal structure across the San Andreas fault, southern California from tele-seismic converted waves, *Earth Planet. Sci. Lett.* **179**, 183-190.

Zhu, L. and H. Kanamori (2000). Moho depth variation in southern California from tele-seismic receiver functions, *J. Geophys. Res*. **105**, 2969-2980.

Appendix. The Directory Structure for RF Calculations

The directory structure and files for calculating nodal receiver functions in the paper are detailed as below.

The main directory is **/Users/lgb/RF**. The main directory looks like as follows:

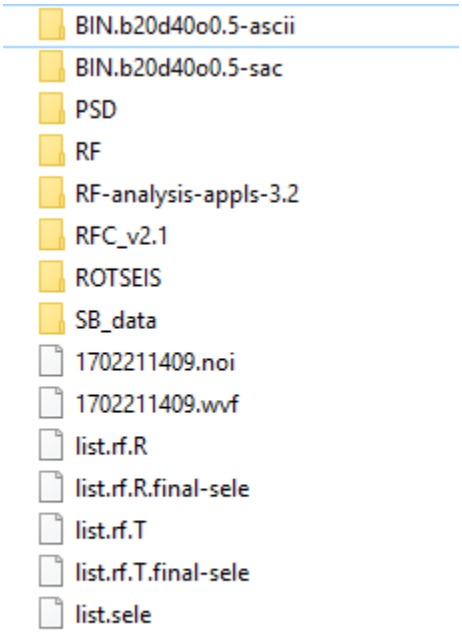

1) /SB_data

Containing the waveforms:

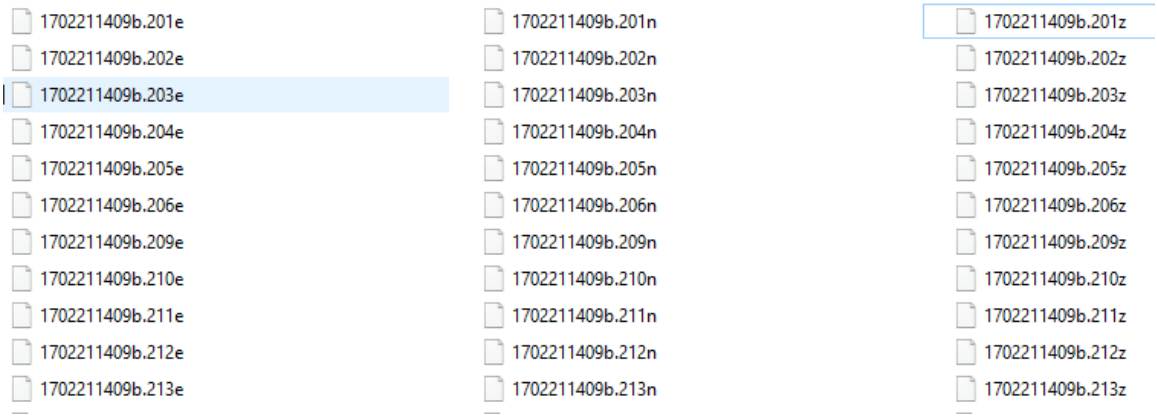

2) /ROTSEIS

Containing the rotated waveforms:

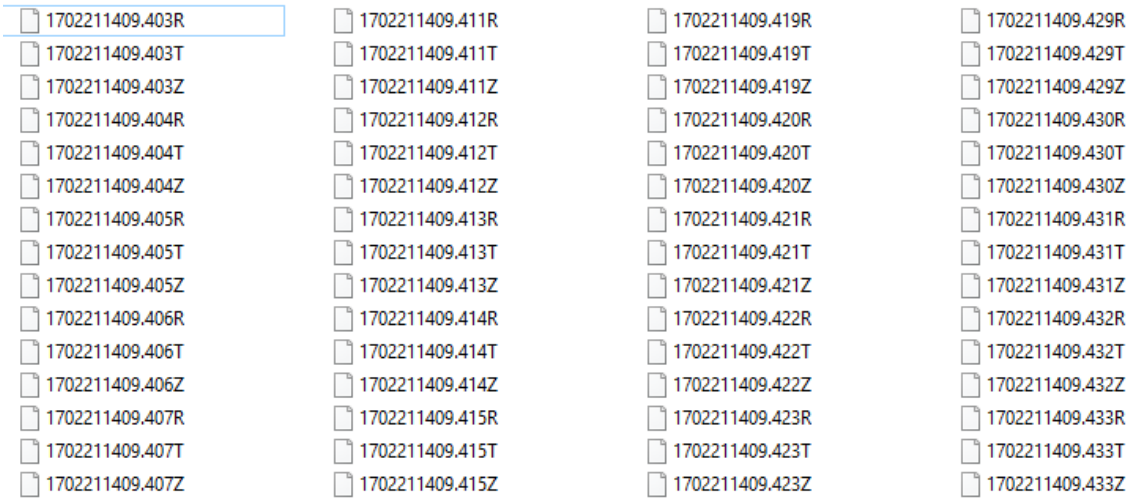

3) /RF

Containing the calculated receiver functions

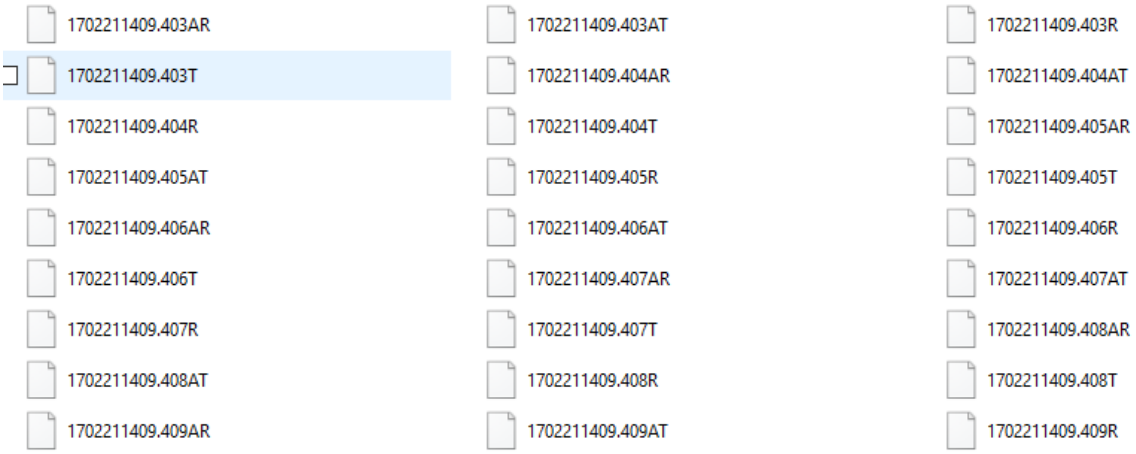

4) /PSD

Containing the calculated Power Spectral Density of the noise

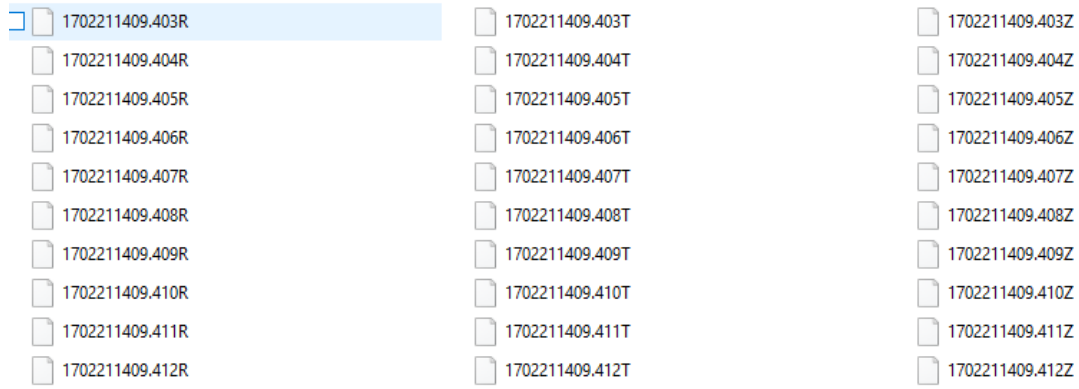

5) /BIN.b20d40o0.5-ascii

Containing the binned receiver functions in ASCII

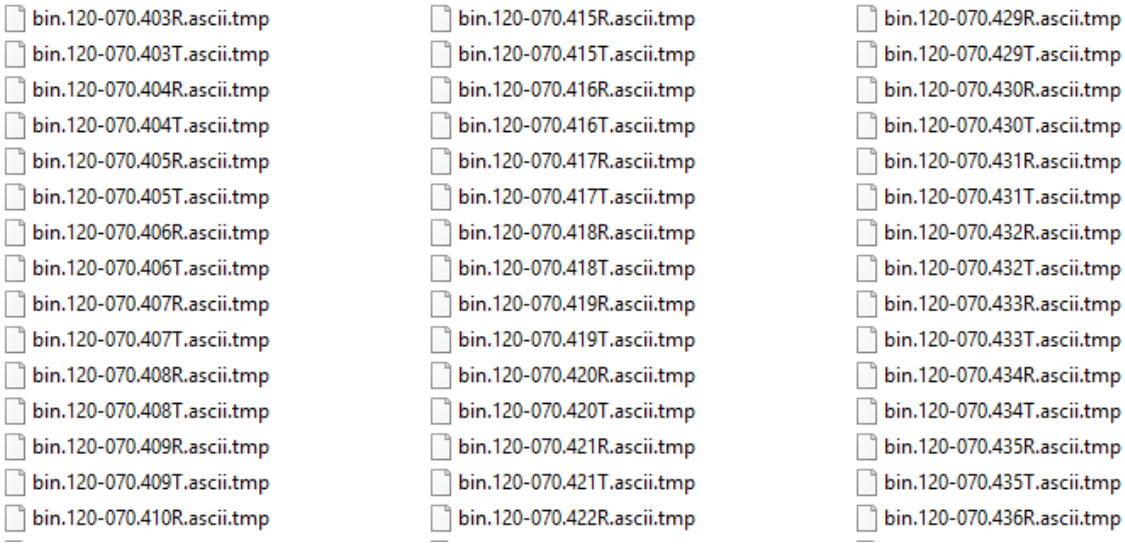

6) /BIN.b20d40o0.5-sac

Containing the binned receiver functions in SAC format

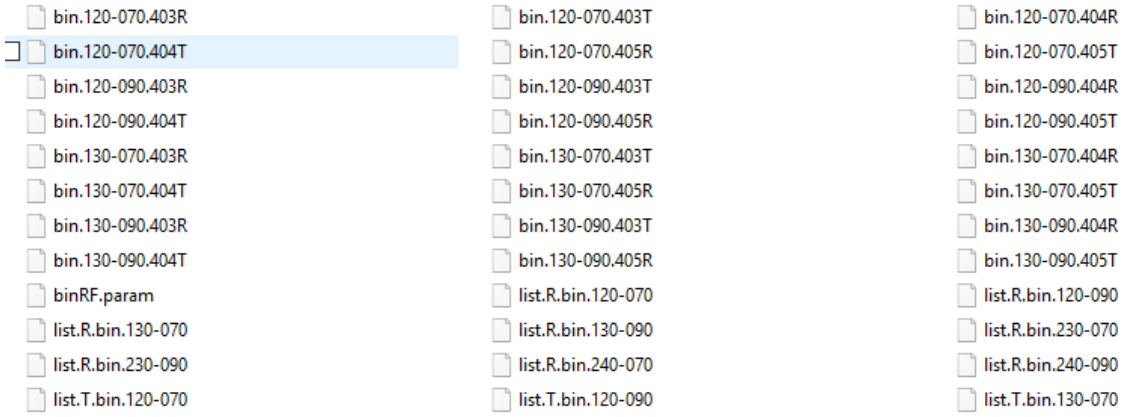

7) **/RF-analysis-appls-3.2** and **/RFC_v2.1** are directories containing the codes.

Vita

Guibao obtained his Bachelor degree from Ocean University of China in 2005 and subsequently obtained his Master's degree from Research Institute of Petroleum Exploration and Development, CNPC, 2008. Both degrees are majored in geophysics. From 2017, he started his graduate study in geophysics at Louisiana State University.